



Combined impacts of climate change and human activities on blue and green water resources in the high-intensity development watershed

Xuejin Tan ¹, Bingjun Liu ^{2*}, Xuezhi Tan ^{2,3*}, Zeqin Huang², Jianyu Fu²

¹ School of Geography and Planning, Sun Yat-sen University, Guangzhou, 510006, PR China

² Center of Water Resources and Environment, School of Civil Engineering, Sun Yat-sen University, Guangzhou, 510275, PR China

³ Southern Marine Science and Engineering Guangdong Laboratory (Zhuhai), Sun Yat-sen University, Zhuhai, 519082, PR China

* Corresponding authors: Bingjun Liu (liubj@mail.sysu.edu.cn)

Xuezhi Tan (tanxuezhi@mail.sysu.edu.cn)



1 Abstract

2 Sustainable management of blue and green water resources is vital for the stability and
3 sustainability of watershed ecosystems. Although there has been extensive attention to blue water
4 (*BW*) which is closely related to human beings, the relevance of green water (*GW*) for ecosystem
5 security is typically disregarded in water resource evaluations. Specifically, there is a scarcity of
6 comprehensive study on the detection and attribution of variation of blue and green water in the
7 Dongjiang River Basin (DRB), an important source for regional water supply in the Guangdong-
8 Hong Kong-Macao Greater Bay Area (GBA) of China. Here we assess the variations of *BW* and
9 *GW* scarcity, quantify the impacts of climate change and land use change on *BW* and *GW* in DRB
10 using a multi-water-flux calibrated Soil and Water Assessment Tool (SWAT). Results show that
11 *BW* and green water storage (*GWS*) in DRB increased slowly with a rate of 0.14 and 0.015 mm a⁻¹,
12 respectively, while green water flow (*GWF*) decreased significantly at a rate of -0.21 mm a⁻¹.
13 The degree of *BW* and *GW* scarcity in DRB is low, and the per capita water resources in more than
14 80% of DRB exceed 1700 m³ capita⁻¹ a⁻¹. Attribution results show that 88.0%, 88.5%, and 39.4%
15 of changes in *BW*, *GWF*, and *GWS* results from climate change, respectively. Both climate change
16 and land use change have decrease *BW*, while climate change (land use change) decrease (increase)
17 *GWF* in DRB. These findings can guide to optimize the allocation of blue and green water
18 resources between upper reach and lower reach areas in DRB and further improve the
19 understanding of blue and green water evolution patterns in humid regions.

20 **Key words:** Blue and green water; Water scarcity; Climate change, Land use change; Water flow;

21 Dongjiang River Basin

22 1 Introduction

23 Land use change (LUCC) and climate variability may alter hydrological processes in



24 watersheds (Chagas et al., 2022; Konapala et al., 2020; Xuezhi Tan et al., 2022), which
25 successively affect variations of regional water resources (Hoek van Dijke et al., 2022; Pokhrel et
26 al., 2021; Stocker et al., 2023), potentially leading to ecosystem degradation and severe water
27 shortage crises (Aghakhani Afshar et al., 2018; Zuo et al., 2015). With the development of society
28 and the economy, there is an increasing need for more water to accommodate human needs,
29 encompassing agricultural, domestic, and industrial water usage. Water scarcity and
30 spatiotemporal mismatch between regional water supply and demand in certain regions are
31 becoming increasingly severe, significantly affecting the sustainable development in these regions
32 (Cook et al., 2014). Quantifying water resources under a changing environment is crucial for
33 guiding efficient and sustainable water use.

34 Previous studies on water resource assessment have explored the effects of climate change
35 and anthropogenic on available water resources, including streamflow (Tan and Gan, 2015; Tan et
36 al., 2023; Xin et al., 2019), baseflow (Ficklin et al., 2016; Tan et al., 2020), lake water (Acero
37 Triana and Ajami, 2022; Tao et al., 2020), and groundwater (Han et al., 2020). Falkenmark and
38 Rockström (2006) introduce a novel perspective on water resource assessment by categorizing
39 water resources into *BW* and *GW*. *BW* is the total of deep aquifers recharge and river streamflow,
40 such as water in lakes, and rivers. Water users such as industries, agriculture, and municipal users
41 can directly utilize *BW*. On the contrary, *GW* is the portion of precipitation that is not streamflow
42 and is temporarily retained in the soil before eventually being released back into the air by



43 evapotranspiration. *GW* encompasses both green water flow (*GW*) and green water storage (*GWS*)
44 (Veettil and Mishra, 2018; Zang and Liu, 2013). Traditional water resource assessments
45 concentrating on available water resources. Only consider *BW* but neglect *GW* (Dai et al., 2022),
46 although *GW* is also essential. *GW* supplies about 80% of total water resources, sustaining crops
47 growth and the sustainable development of forest and grasslands ecosystems in arid regions or
48 during dry seasons (Li et al., 2018; Schuol et al., 2008). The green water scarcity can lead to
49 ecosystem degradation and intensify competition between human needs and ecosystems for water
50 resources (Falkenmark et al., 2003; Veettil and Mishra, 2018). Compared to traditional streamflow
51 assessment methods, water resource scarcity assessment methods based on the framework of *BW*
52 and *GW* are more appropriate for maintaining sustainable water resource management (Cooper et
53 al., 2022; Liu et al., 2017). Recently, some researches have characterized water scarcity by
54 assessing variations of *BW* and *GW*. Veettil and Mishra (2020) assess blue water scarcity and green
55 water scarcity to show the water security status of counties in the United States. Hoekstra et al.
56 (2012) uses the concept of *BW* footprint to study water scarcity issues. Schyns et al. (2019) uses
57 the conception of *GW* footprint to investigate green water scarcity and found that the increasingly
58 severe shortage of *GW* poses a significant threat to natural ecosystems.

59 Impacts of climate change and anthropogenic on the hydrological cycle processes in
60 watersheds have attracted widespread attention (Chouchane et al., 2020; Cooper et al., 2022;
61 Sherwood and Fu, 2014; Tan and Gan, 2015; Xuejin Tan et al., 2022; Veettil and Mishra, 2016).



62 Changes in land use alter the underlying surface conditions. For example, afforestation or
63 deforestation may exacerbate or alleviate global or regional climate change, and thus affect
64 hydrological cycle processes (Bai et al., 2020; Lian et al., 2020; Qiu et al., 2023). Changes in land
65 use often lead to alterations in land-atmosphere interactions, and vegetation cover changes are
66 essential for regulating climate systems and land ecosystems (Foley et al., 2005; Huang et al.,
67 2020). Large-scale greening could modify geophysical interactions between the atmosphere and
68 the ground, impacting larger or local regional hydrological cycles. Land degradation (Walters and
69 Babbar-Sebens, 2016), deforestation (Lee et al., 2011), and urbanization (Mohan and Kandya,
70 2015; Zhang et al., 2018) also have far-reaching effects on climate and hydrological cycle.

71 Climate change is also crucial to the variations in *BW* and *GW* resources. Precipitation is the
72 source of *BW* and *GW*, and factors such as temperature, solar radiation, and potential
73 evapotranspiration significantly influence the changes of *BW* and *GW* in the basins, especially in
74 *GWF* (Pandey et al., 2019; Schewe et al., 2014). For a single watershed, *BW* depends directly on
75 precipitation and evapotranspiration (*GWF*) (Shen et al., 2017; Vano et al., 2012). Furthermore,
76 precipitation intensity can have a significant impact on the redistribution of precipitation and *BW*,
77 as well as *GW*, by altering infiltration and runoff generation processes (Eekhout et al., 2018;
78 Nearing et al., 2005). Therefore, it is crucial to quantify the effects of climate change and LUCC
79 on *BW* and *GW* resources in a basin for effective water resource planning and management.

80 The Dongjiang River Basin (DRB) is a crucial water source for core cities in GBA, such as



81 Shenzhen, Hong Kong, and Huizhou. Given the significant *BW* demand from agriculture, urban
82 areas, and industry, as well as the *GW* demand from over 18,000 km² of forested land, the water
83 resource stress in DRB is extremely high, although DRB is located in the wet South China (Liu et
84 al., 2018). The growing mismatch between increasing water demand and decreasing water supply,
85 along with seasonal and pollution-induced water scarcity issues, is becoming increasingly
86 prominent (Yang et al., 2018). Currently, the majority of studies on water resources of DRB focus
87 on changes and scarcity of surface water and groundwater (*BW*) while overlook the critical role
88 and spatiotemporal variations of *GW* (Huang et al., 2022; Jiang et al., 2023; Jiefeng Wu et al.,
89 2021). With the high-intensity urbanization and climate change in DRB, changes of *BW* and *GW*
90 resource in DRB remain unknowns.

91 This research aims to analyze the influence of climate change and LUCC on *BW* and *GW* in
92 DRB. The objectives of this research are (a) to build the SWAT model for DRB, (b) to
93 quantitatively evaluate the spatial and temporal variation of *BW* and *GW* in DRB, (c) to assess the
94 status of water scarcity in DRB using the framework of *BW* and *GW* resources, (d) to estimate the
95 effects of climate change and LUCC on *BW* and *GW* in DRB.

96 **2 Materials and methods**

97 **2.1 Study area**

98 The Dongjiang River serves as a important tributary of the Pearl River, positioned between

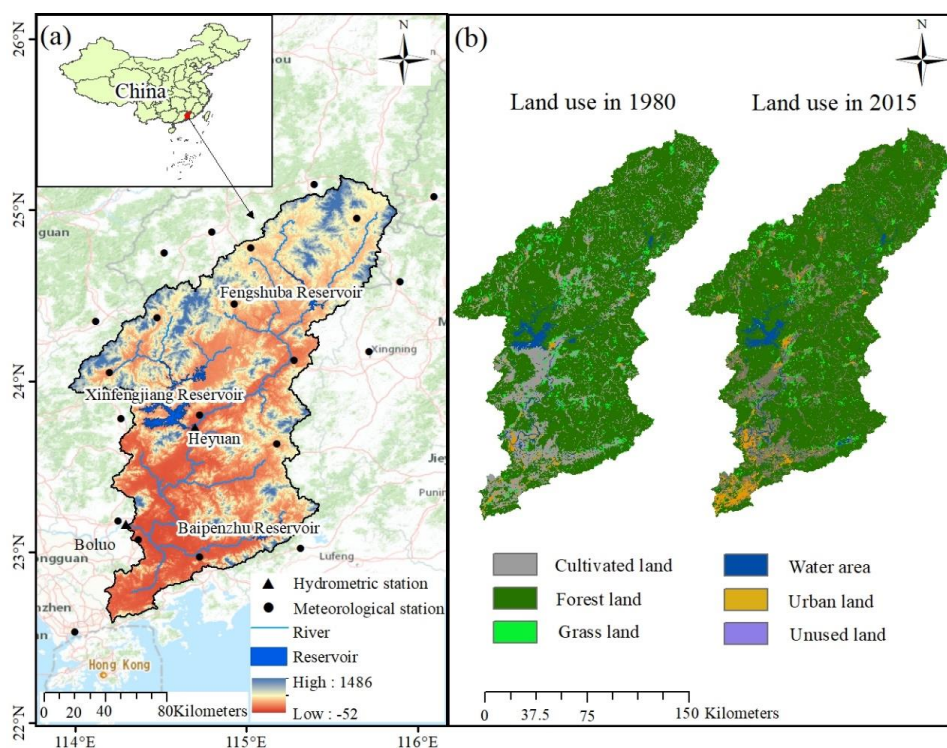


99 longitude 113°25'-115°52'E and latitude 22°26'-25°12'N. It originates in Xunwu County, Jiangxi
100 Province, flows through Jiangxi and Guangdong provinces, and goes across major cities including
101 Longchuan, Heyuan, Dongguan, and Shenzhen. The main stem of the Dongjiang River spans a
102 total length of 562 km, covering a watershed area of 3.5×10^4 km². DRB is situated within the
103 subtropical monsoon climate zone with adequate precipitation and high temperatures. The average
104 annual precipitation ranges from 1500-2400 mm, and the average temperature of the basin is
105 approximately 21°C (Jiefeng Wu et al., 2019). The altitude of the basin decreases from northeast
106 to southwest. The upper reaches of DRB are dominated by mountains and hills, the middle reaches
107 of DRB are dominated by hills and plains, and the lower reaches of DRB are dominated by plains.

108 Previous hydrological simulation studies of DRB mainly use the Boluo hydrometric station
109 as the outlet of the watershed (He et al., 2013; Jiefeng Wu et al., 2019), so this research only
110 analyze the area of DRB where water flows to the Boluo station (Fig. 1). The Boluo hydrometric
111 station is the main control station in the lower reaches of the Dongjiang. The Boluo hydrometric
112 station occupy a drainage area of 25,325 km², which is 71.7% of the overall DRB. Since the 1950s,
113 more than 896 reservoirs, ponds, dams, and other water conservancy facilities have been
114 constructed in DRB. Among them, the Baipenzhu Reservoir, Fengshuiba Reservoir, and
115 Xinfengjiang Reservoir are the main reservoirs in the basin with a cumulative storage capacity of
116 approximately 17,048 million m³. The Dongjiang-Shenzhen Water Supply Project constructed in
117 1964 diverts water from the Dongjiang River to Shenzhen and Hong Kong for providing fresh



118 water resources for municipal use. Over 70% of Hong Kong's freshwater supply comes from the
119 Dongjiang River. Therefore, it is crucial to comprehend the shifts in water resources within DRB
120 for projecting future available water resources for the development of GBA.



121
122 Figure 1. Location and characteristics of the study area: (a) location of the watershed, spatial distribution of the
123 hydrometeorological stations, and digital elevation model (Farr et al., 2007), (b) land use map (Xu et al.,
124 2018).

125 2.2 Methodology

126 2.2.1 SWAT model

127 The SWAT model was adopted to simulating hydrological processes and estimating the
128 volume of *BW* and *GW* for DRB (Arnold et al., 1998; Neitsch et al., 2002). The SWAT model is



129 widely applied to simulate streamflow and surface runoff (Arshad et al., 2022; Martínez-Salvador
130 and Conesa-García, 2020; Nie et al., 2023). The SWAT model is also widely utilized for exploring
131 the changes of *BW* and *GW* (Dai et al., 2022; Liang et al., 2018; Schuol et al., 2008).

132 In SWAT modelling, DRB was divided into 63 sub-basins, and each sub-basin was then
133 categorized into Hydrologic Response Units (HRUs) depending on land use, soils, and slope.

134 2.2.2 Model calibration and validation

135 In order to reduce the influence of hydraulic engineering, the SWAT model was calibrated
136 and validated utilizing monthly restored natural streamflow at the Boluo and Heyuan hydrometric
137 stations. The optimum hydrological parameters were shown in Table 1. All selected parameters are
138 automatically calibrated with 500 simulations via SWAT-CUP. The warm-up period for model
139 simulations is the first two years of the simulation period. Restored natural streamflow in 1970-
140 1979 was used to calibrate the model, and monthly time series of restored natural streamflow, *ET*
141 from GLEAM, and soil moisture from ERA5 during 1980-1989 were used to validate the model.
142 The calibration period for this research was 1970-1979, and the validation period was 1980-1989.
143 Three metrics, including the determination coefficient (R^2), the percentage bias (*PBIAS*), Nash-
144 Sutcliffe efficiency (*NSE*) were applied to evaluate simulation performance of SWAT model:

$$145 \quad NSE = 1 - \frac{\sum_{i=1}^n (Q_{nat} - Q_{sim})^2}{\sum_{i=1}^n (Q_{nat} - Q_{ave})^2} \quad (1)$$



146
$$PBIAS = \frac{\overline{Q_{sim}} - Q_{ave}}{Q_{ave}} \times 100 \quad (2)$$

147
$$R^2 = \left[\frac{\sum_{i=1}^n (Q_{nat} - Q_{ave})(Q_{sim} - \overline{Q_{sim}})}{\sqrt{\sum_{i=1}^n (Q_{nat} - Q_{ave})^2 \sum_{i=1}^n (Q_{sim} - \overline{Q_{sim}})^2}} \right]^2 \quad (3)$$

148

149 where Q_{nat} , Q_{ave} , Q_{sim} , and $\overline{Q_{sim}}$ are monthly natural streamflow, mean monthly natural
 150 streamflow, simulated streamflow, and mean monthly simulated streamflow, respectively, and n is
 151 the time step.

152 Table 1 Range of the main parameters and their optimal values in the calibration period

Parameter	Calibration type	Initial range	Best calibrated value
GW_REVAP.gw	V	0.19-0.2	0.199
GWQMN.gw	V	493-1247	916.493
SLSUBBSN.hru	R	2.6-5.7	2.804
ESCO.hru	V	0.89-0.97	0.901
CN2.mgt	R	0.14-0.27	0.209
CH_K2.rte	V	0.38-1.16	0.926
ALPHA_BNK.rte	V	0.12-0.18	0.165
SOL_AWC.sol	R	0.3-0.6	0.598
SOL_K.sol	R	0.32-0.69	0.669
CH_K1.sub	V	0-0.15	0.0295

Note: The symbols of V and R denote a replacement and a relative change to the default parameter value, respectively.

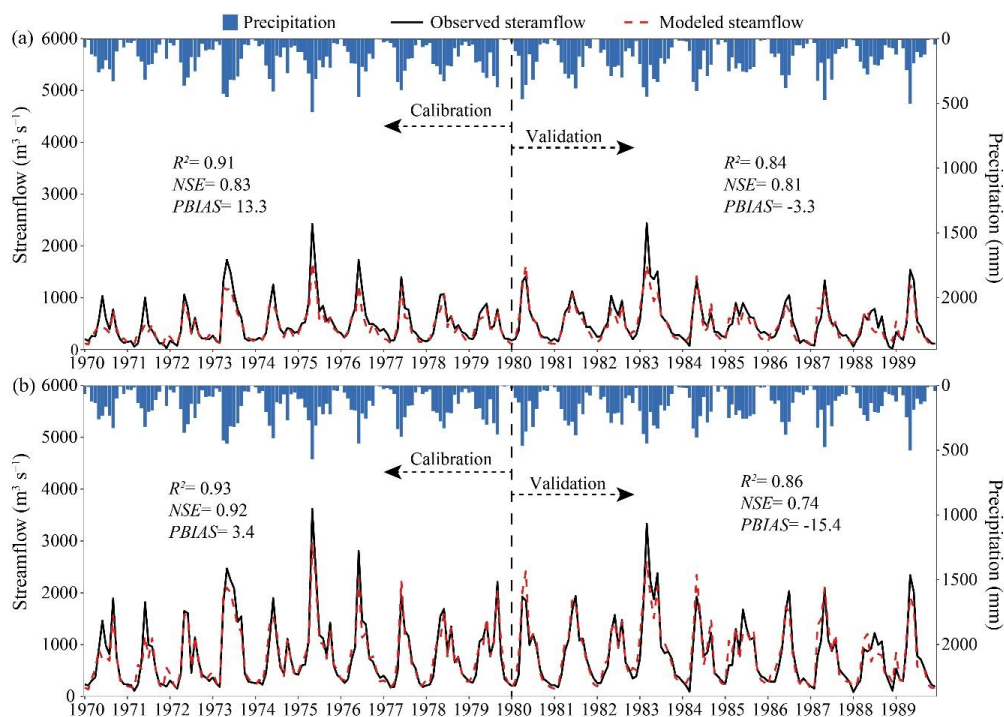
153 This study reconstructed the natural monthly streamflow series of the basin by combining the
 154 inflow and outflow of the three major reservoirs (Xinfengjiang Reservoir, Fengshuba Reservoir,
 155 and Baipenzhu Reservoir) in DRB, based on the watershed water balance (Tu et al., 2018):

156
$$Q_{nat} = Q_o + \Delta Q = Q_o + Q_{in} - Q_{out} \quad (4)$$



157 where ΔQ is the total reduced water volume, Q_o , Q_{in} , and Q_{out} are the observed streamflow,
158 reservoir inflow, and reservoir outflow, respectively.

159 Overall, the SWAT model shows sufficient accuracies in simulating streamflow, actual
160 evapotranspiration, and soil moisture changes in DRB and can better simulate both seasonal and
161 interannual changes in streamflow. During the calibration period, both stations achieved R^2 above
162 0.9, NSE exceeding 0.8, and $PBIAS$ less than 14% (Fig. 2). Both stations had simulation streamflow
163 R^2 greater than 0.8 during the validation period. The NSE for streamflow simulation at the Heyuan
164 station and Boluo station of the validation were 0.81 and 0.74, respectively. The model performed
165 well in simulating the ET and soil moisture. Since the GLEAM ET data and ERA5 soil moisture
166 data are raster data of spatial resolution of $0.25 \times 0.25^\circ$, considering the influence of data accuracy
167 on the results, this study uses the watershed scale to validate the simulation results of ET and soil
168 moisture. In the validation period, the R^2 and NSE for the simulation of evapotranspiration were
169 0.92 and 0.8, respectively (Fig. S1), while the R^2 and the NSE for the soil moisture simulation were
170 both greater than 0.6. These validation results show that the model can be used to simulate
171 hydrological regimes in DRB.



172
173 Figure 2. Simulated and observed monthly streamflow at the (a) Heyuan and (b) Boluo gauge stations
174 during calibration and validation periods.

175 2.3 Scenario design and simulation

176 Three scenarios were formulated to assess the impacts of climate change and LUCC on *BW*
177 and *GW* by changing climate conditions (land use) while holding land use (climate conditions) for
178 each scenario simulation (Table 2). The LUCC for simulating the influences of climate change on
179 hydrological cycle (S2-S1), while climate conditions change for simulating the influences of
180 LUCC on hydrological cycle (S3-S2). The climate conditions and the land use were altered when
181 assessing the joint influences of climate change and LUCC (S3-S1).

182 Table 2 Scenario settings for the simulation of effects of climate change and LUCC on blue and green water



Scenarios	Land use	Climate period	Combined effects	Land use change effects	Climate change effects
S1	1980	1970-1993			
S2	1980	1994-2017			S2-S1
S3	2015	1994-2017	S3-S1	S3-S2	

183 2.4 Calculation of blue and green water and water security indicators

184 2.4.1 Blue and green water scarcity

185 Blue water scarcity (*BWSC*) is determined by the quotient of *BW* withdrawal and availability.
186 The estimation of *BW* withdrawals (*BWR*) in this study involved the multiplication of the aggregate
187 population in each sub-basin by the combined water consumption per person (Liang et al., 2020).
188 The population of each sub-basin was extracted from the population raster data. *BW* availability
189 (*BWA*) represents the quantity of water that can be utilized without negatively impacting the river
190 ecosystems. Exhaustive exploitation of *BW* in rivers may adversely impacts river ecosystems.
191 Previous studies have generally used environmental flow requirements (*EFQ*) as a suitable metric
192 for sustaining robust ecosystems (Honrado et al., 2013). According to the study of Richter (2010)
193 and Richter et al. (2012), extracting more than 20% of the water from rivers may result in
194 ecological degradation. Therefore, 20% of streamflow can be deemed *BW* and used for water
195 supply. (Veettil and Mishra, 2016). The calculation of *EFR*, *BWA*, and *BWSC* are as follows:

$$196 \quad EFQ_{(a,t)} = 0.8 \times Q_{\text{mean}(a,t)} \quad (6)$$

197 where $EFQ_{(a,t)}$ is the *EFQ* for sub-basin 'a' during time 't'; Q_{mean} is the long-term monthly average



198 streamflow.

$$199 \quad BWA_{(a,t)} = Q_{(a,t)} - EFQ_{(a,t)} \quad (7)$$

$$200 \quad BWSC = BWR/BWA \quad (8)$$

201 Green water scarcity (*GWSC*) is defined as the ratio between green water footprint (*GWFO*)
202 and green water availability (*GWA*). The *GWFO* denotes the actual evapotranspiration from the
203 watershed. *GWA* is the soil moisture that is available for evapotranspiration and vegetation
204 transpiration and is equal to the initial soil moisture (Liang et al., 2020). The *GWSC* can be
205 formulated as:

$$206 \quad GWSC_{(a,t)} = GWFO_{(a,t)} / GWA_{(a,t)} \quad (9)$$

207 where *GWSC* is green water scarcity; *GWFO*_(*x*,*t*) is the actual evapotranspiration; *GWA*_(*a*,*t*) is initial
208 soil moisture.

209 2.4.2 Regional water stress

210 The Falkenmark index (*FLK*) (Falkenmark et al., 1989) is a widely used measures of water
211 stress, defined as the proportion of *BWA* to the overall population. The Falkenmark index is
212 classified into no stress, stress, scarcity, and absolutely scarcity based on per capita water use.
213 Absolute scarcity is regarded to occur in areas where the indicator threshold is less than 500 m³
214 capita⁻¹ a⁻¹, and no stress is thought to occur in areas where the threshold is larger than 1700 m³
215 capita⁻¹ a⁻¹.



216 2.5 Calculation of relative contribution

217 The influences of climate change and LUCC on the changes of blue and green water in
218 different periods are evaluated utilizing the relative contribution rate in this research (Li et al.,
219 2021):

220 Climate change contribution to *BW* and *GW* change is estimated by:

$$221 \quad CR_c = \frac{|X_2 - X_1|}{|X_2 - X_1| + |X_3 - X_2|} \times 100\% \quad (10)$$

222 where X is the amount of *BW* or *GWF* and *GWS* for each scenario.

223 The contribution of LUCC to *BW* and *GW* change is estimated by:

$$224 \quad CR_L = \frac{|X_3 - X_2|}{|X_3 - X_2| + |X_2 - X_1|} \times 100\% \quad (11)$$

225 2.6 Data

226 The dataset used in this study consists of three parts: (1) hydrometeorological data, (2)
227 geospatial data encompassing DEM, soil type, and land use, and (3) socioeconomic data
228 encompassing per capita water consumption and population data.

229 Observed monthly streamflow data of the two hydrological stations in the study were
230 collected for the years 1970-2000 from Boluo Station and Heyuan Station, and the observed
231 streamflow time series of these two hydrological stations are of no missing data. Monthly inflow
232 and outflow data of the three major reservoirs in DRB were also collected. All hydrologic data



233 were obtained from the Guangdong Provincial Hydrological Bureau. Meteorological data of daily
234 precipitation, temperature, and other meteorological data for 1968-2017 from 21 Meteorological
235 stations in the watershed were obtained from the National Meteorological Information Center of
236 the China Meteorological Administration. Monthly actual *ET* data for SWAT model validation was
237 obtained from the Amsterdam Evapotranspiration Model dataset with a spatial resolution of 0.25°
238 $\times 0.25^\circ$ (Martens et al., 2017). Monthly soil moisture data for SWAT model validation was obtained
239 from the European Center for Medium-Range Weather Forecasts ERA5-land dataset with a spatial
240 resolution of $0.1^\circ \times 0.1^\circ$ (Muñoz Sabater, 2019). The actual evapotranspiration and soil moisture
241 of the watershed equals to the average of all grids included in DRB.

242 The 90 meter resolution DEM data and 30 meter resolution land use data at ten-year intervals
243 (i.e., 1980, 1990, 2000, 2010, 2015) are obtained from the Data Center for Resources and
244 Environmental Sciences of the Chinese Academy of Sciences (Xu et al., 2018). Soil data is
245 obtained from the 1-km resolution Harmonized World Soil Database dataset from the Food and
246 Agriculture Organization of the United Nations (Fischer et al., 2008).

247 The annual per capita integrated water consumption data of DRB from 2000-2017 was
248 acquired from the Water Resources Bulletin of Guangdong Province. The population data in 2000,
249 2005, 2010, and 2015 was obtained from the 1×1 km spatial raster data of the Resource and
250 Environment Science and Data Center of the Chinese Academy of Sciences (Xu, 2017).



251 **3 Results**

252 3.1 LUCC and Climate variability in DRB

253 LUCC in DRB is mainly the decrease of cultivated land and the increase of urban land. The
 254 land use in DRB primarily consisted of forest land (18,875-18833 km²), which is more than 70%
 255 of DRB. From 1980 to 2015, the urban land and water areas showed an increase of 469.4 km²
 256 (137%) and 17.4 km² (2.8%), while the grass land, cultivated land, and forest land showed a
 257 decrease of 41.3 (4.3%), 487.5 (10.8%), and 42.1 km² (0.2%), respectively (Table 3).

258 Table 3 Land use transfer matrix in DRB from 1980 to 2015

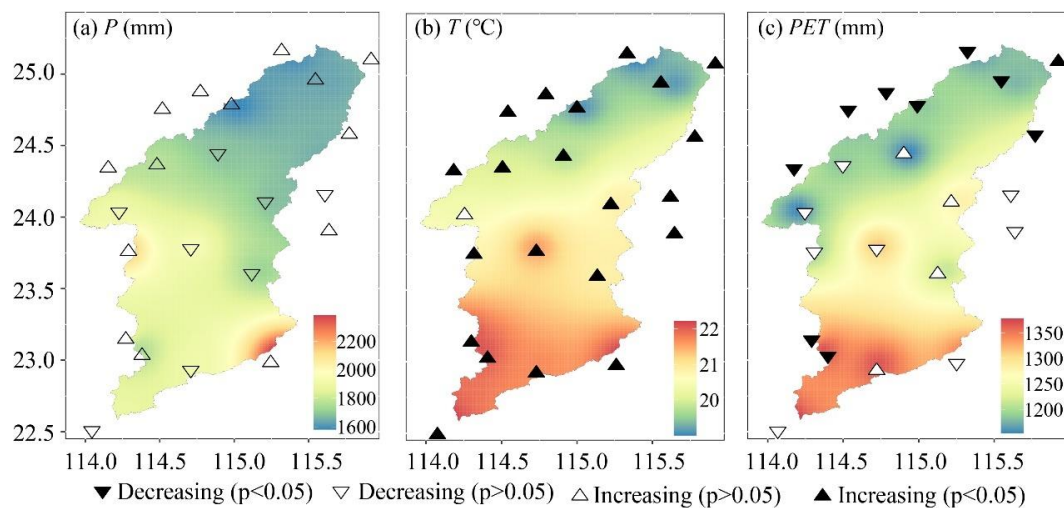
Land use type	2015						1980 total (km ²)
	Grass Land (km ²)	Urban land (km ²)	Cultivated Land (km ²)	Forest land (km ²)	Water area (km ²)	Unused land (km ²)	
1980 Grass land	795.6	29.9	18.3	123.5	2.5	0.0	969.7
Urban land	0.6	319.6	12.4	7.6	2.3	0.0	342.4
Cultivated land	19.0	269.8	3771.7	427.9	40.4	0.03	4528.8
Forest land	110.7	183.7	226.2	18278.7	33.1	0.02	18832.5
Water area	2.5	8.9	12.7	36.8	551.0	0.00	611.9
Unused land	0.0	0.0	0.02	0.03	0.00	0.45	0.51
2015 total	928.4	811.9	4041.3	18874.5	629.2	0.51	25285.8

259 DRB exhibited significant regional differences in multi-year average precipitation,
 260 temperature, and potential evapotranspiration. The precipitation exhibited an increasing trend from
 261 the central to the south and north of DRB. The temperature and potential evapotranspiration
 262 showed an overall distribution pattern of greater values in the south and minor values in the north



263 of DRB (Fig. 3). The multi-year average precipitation for the entire of DRB was 1790.1 mm, with
264 annual precipitation ranging from 1236.2-2567.5 mm. The regions with the highest multi-year
265 average annual precipitation are located in the southeast of DRB, where annual precipitation
266 exceeds 2200 mm, while the regions with the lowest precipitation are in the northeastern of the
267 watershed. The average annual temperature in DRB ranged from 19.5-21.3 °C, and the average
268 annual potential evapotranspiration ranged from 1101.5-1320.6 mm. The south of DRB is
269 predominantly urban, characterized by the urban heat island effect, while the north of DRB is
270 mountainous with higher elevations, leading to the spatial distribution of temperatures.

271 The average temperature and potential evapotranspiration at DRB meteorological stations
272 exhibited significant variations, while precipitation showed a relatively minor trend (Fig. 3).
273 Overall, basin-averaged precipitation and potential evapotranspiration showed a non-significant
274 decreasing trend, while temperatures showed a significant increasing trend. There was no
275 significant change trend of precipitation for all stations in DRB (Fig. 3a). Twenty out of 21
276 meteorological stations in the region showed statistically significant increasing trends in average
277 temperature, indicating a warming trend (Fig. 3b). Nine stations showed a significant decreasing
278 trend in potential evapotranspiration, primarily located in northern DRB (Fig. 3c).



280 Figure 3. Spatial distribution of annual mean (a) precipitation, (b) temperature, (c) potential
281 evapotranspiration in DRB from 1960-2017. Each triangle represents the Mann-Kendall test result at a
282 meteorological station.

283 3.2 Blue and green water resources

284 The average annual *BW* and *GW* were 1240.8 and 840.7 mm, respectively. The DRB water
285 resources were dominated by *BW*, representing 60.1% of the total water resources, and *BW* was
286 1.48 times higher than that of *GW* resources. The average *GWF* and *GWS* were 689.3 and 151.4
287 mm, respectively.

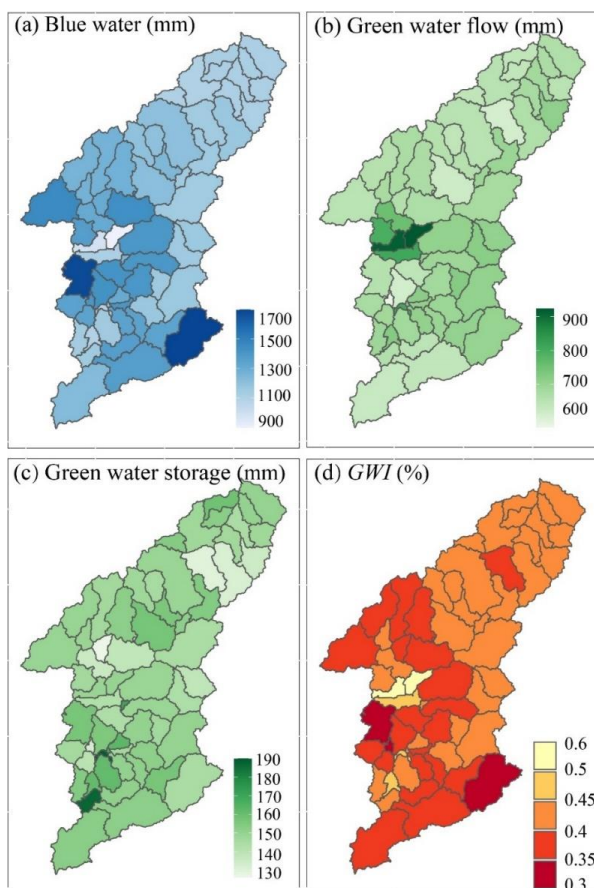
288 The annual *BW* resources in the sub-basins of DRB ranged from 893.7-1990 mm, showing
289 an increasing trend from the central to the south and north of DRB, aligning with the spatial
290 distribution of precipitation (Fig. 4a). The regions with abundant *BW* resources are situated in the
291 central and southeast parts of DRB (>1300 mm), and the *BW* in the upper reaches is comparatively
292 low (<1100 mm). Differences in the spatial distribution of *BW* are primarily caused by differences



293 in the spatial distribution of precipitation. Overall, the *GWF* and *GWS* are more evenly distributed
294 in the sub-basins than *BW*. The annual *GWF* in the sub-basins of DRB ranged from 573.6-923.6
295 mm. The sub-basins with higher *GWF* are primarily located in the Xinfengjiang reservoir area in
296 the middle reaches (>700 mm), while the low *GWF* sub-basins are situated in the southwest of
297 DRB (<600 mm) (Fig. 4b). The land use in the sub-basins where Xinfengjiang Reservoir is located
298 is primarily water areas, with a higher water evaporation rate than other regions, resulting in a
299 greater *GWF* in this area than in other regions. The annual *GWS* in the sub-basins of DRB ranged
300 from 126-190.6 mm. The sub-basins with higher *GWS* are mainly located in the lower part of DRB
301 (>150 mm) (Fig. 4c). The distribution pattern of *GWS* resources has a great relationship with the
302 soil type of the watershed. The upper reaches and the northwestern part of the watershed are mostly
303 red soil, while the middle and lower reaches are dominated by reddish soil. Reddish soil has a
304 smaller water storage capacity than red soil, loses water faster, and has weaker water conservation
305 and water supply performance than red soil. This is the primary factor for the north-south
306 discrepancies in the amount of *GWS* resources in DRB. In addition, the southern region is mostly
307 of large and medium-sized cities. As urban construction land expands, the land use type in the
308 region has gradually changed to urban land, industrial land, etc., and the solidification of road
309 surfaces has reduced the area of bare soil in the region, resulting in a decrease in *GWS* resources.
310 The annual *GWI* (Fig. 4d) showed a spatial pattern opposite to *BW*, decreasing from 0.45 in the
311 upper reaches to 0.3 in the lower reaches. The highest *GWI* is found in the upper reaches, which is



312 due to the relatively low rainfall in the upper reaches and the lush vegetation, with significant plant
313 interception and transpiration, resulting in a higher proportion of total evapotranspiration than in
314 the middle and lower reaches. The central part of the basin has the highest precipitation, leading
315 to a lower *GWI*. The southern part of the watershed has the highest temperature, and
316 evapotranspiration is high. Meanwhile, the lower reaches have a large proportion of agricultural
317 and urban land, and crop irrigation can increase evapotranspiration.

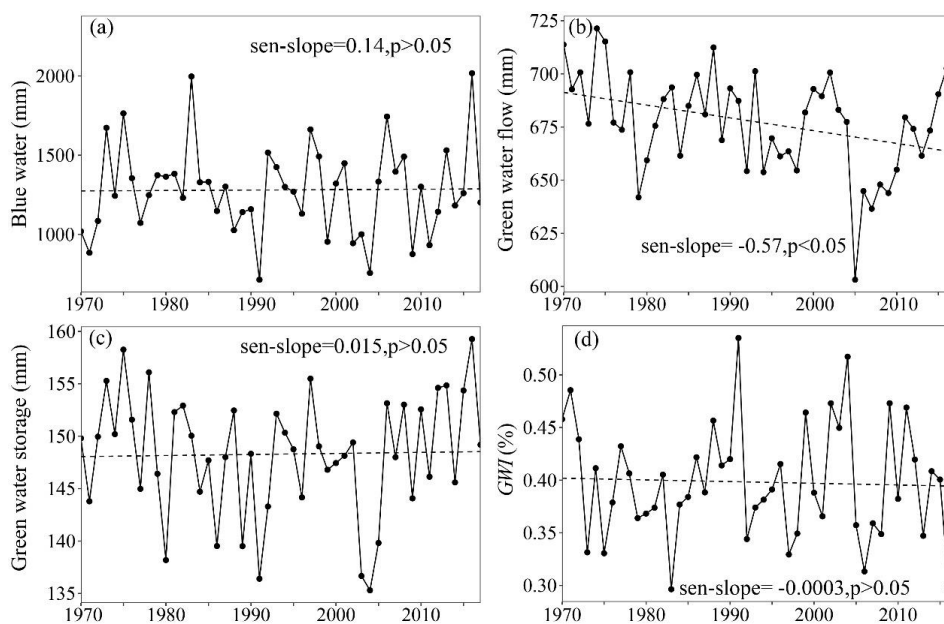


318
319 Figure 4. Spatial distribution of mean (a) *BW*, (b) *GWF*, (c) *GWS*, (d) *GWI* in DRB over during 1970-2017.

320 In DRB, there was no significant increasing trend in either *BW* or *GWS*, while *GWF*



321 exhibited a significant decreasing trend. The annual trend rate of BW in DRB was 0.14 mm a⁻¹,
322 with an annual fluctuation range of 713.6–2017.5 mm during 1970–2017. The minimum BW
323 occurred in 1991, while the maximum was recorded in 2016 (Fig. 5a). The GWF in DRB from
324 1970 to 2017 exhibited a significant decreasing trend (-0.57 mm a⁻¹) (Fig. 5b). The minimum
325 GWF occurred in 2005 (603.1 mm), while the maximum was recorded in 1974 (721.3 mm). In
326 contrast, the GWS in DRB from 1970 to 2017 has been slowly increasing at a rate of 0.015 mm a⁻¹
327 (Fig. 5c). The annual fluctuation in GWS was smaller than BW and GWF. The GWI in DRB
328 from 1970 to 2017 showed no significant decreasing trend at a rate of -0.0003 % a⁻¹ ($p > 0.05$) (Fig.
329 5d), implying that the redistribution of precipitation in DRB might change slowly.



330

331 Figure 5. Interannual variation of (a) *BW*, (b) *GWF*, (c) *GWS*, (d) *GWI* in DRB during 1970–2017.



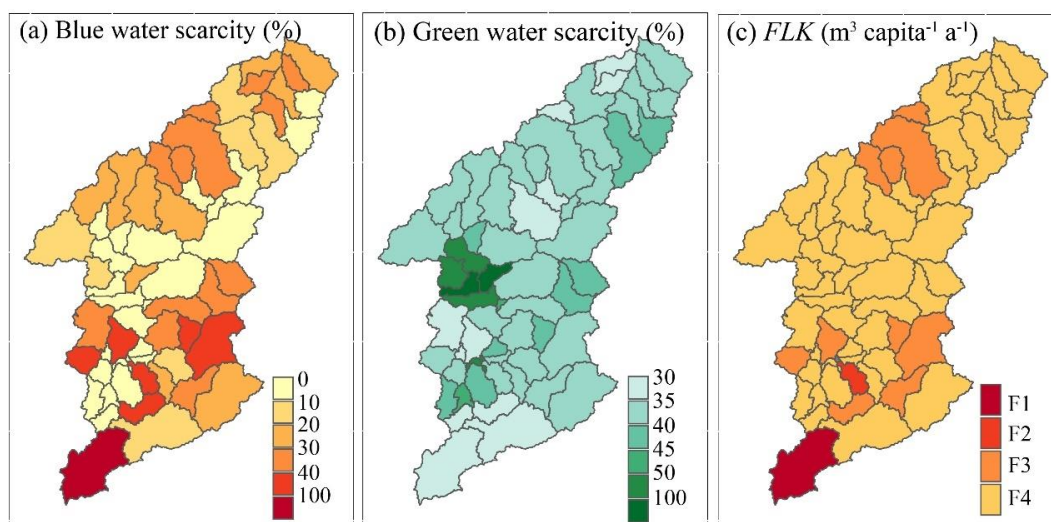
332 3.3 Blue and green water scarcity

333 The average blue water scarcity level in DRB was low (22.4%) during 1970-2017. The blue
334 water scarcity levels in various sub-basins ranged from 0.1-206%. The multi-year average blue
335 water scarcity, except for one sub-basin in the southwest, was all low (<100%) (Fig. 6a). This
336 indicates that blue water scarcity is not common in DRB at the annual scale. Regions with
337 relatively high blue water scarcity (>20%) are mostly situated in the upper reaches of various
338 tributaries within the watershed, where river streamflow is relatively small. The area with the
339 highest blue water scarcity (206%) is located in the 63rd sub-basin of Shenzhen and Huizhou,
340 reaching a moderate level of blue water scarcity. This region has a large population, with a much
341 higher blue water demand than other areas. Additionally, this sub-basin is situated in the upper
342 reaches of the primary tributary of DRB, resulting in a limited supply of *BW* resources. Although
343 the northern parts of sub-basins 55, 56, and 61 have large populations, these sub-basins are situated
344 in the downstream of the main Dongjiang River, with a higher streamflow, leading to lower *BWSC*
345 levels. The average *GWSC* in the entire basin from 1970-2017 was low (41.4%). The blue water
346 scarcity levels in various sub-basins ranged from 31-104%. The vegetation cover in DRB is high,
347 and DRB is thus of relatively high rates of vegetation transpiration and interception evaporation.
348 The basin experiences a *GWSC* of nearly 50%, indicating a potential occurrence of *GWSC*. The
349 areas with higher *GWSC* are primarily situated in the middle reaches for DRB (Fig. 6b), where
350 water surface evaporation is high, resulting in their *GWSC* exceeding 100%. The evaporated water



351 in these areas originates from the reservoirs, not the soil, leading to an overestimation of the *GWSC*
352 in these sub-basins.

353 Furthermore, the *FLK* index was also used to quantify population-driven water resource
354 scarcity. F1-F4 represent absolute scarcity, scarcity, stress, and no stress, respectively. The results
355 showed that most regions in DRB have no water scarcity pressure (Fig. 6c). However, the 63rd
356 sub-basin experienced absolute water scarcity, and the 52nd sub-basin experienced water scarcity.
357 There were six lower reaches sub-basins and four upper reaches sub-basins facing water stress.
358 DRB receives ample precipitation, resulting in a relatively large river flow, generally leading to a
359 higher *FLK* index. As a result, the basin faces lower water resource pressure.

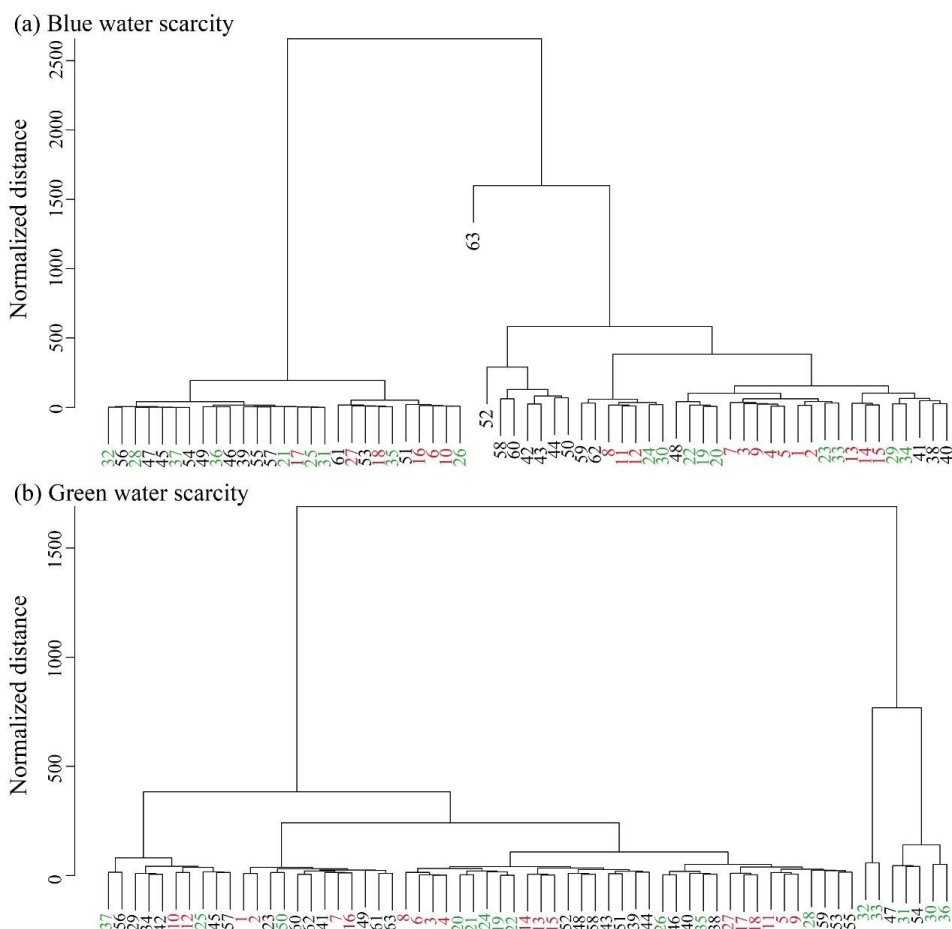


360
361 Figure 6. Spatial distribution of mean (a) *BWSC*, (b) *GWSC*, and (c) *FLK* index in DRB over during 1970-
362 2017.

363 This study also further identified hotspots of *BWSC* and *GWSC* in DRB by hierarchical
364 clustering of *BWSC* and *GWSC* in each sub-basin. Figure 7 shows the clustering tree results for



365 *BWSC* and *GWSC*. When the standardized distance was set to 500, all sub-basins could be divided
366 into four categories according to blue water scarcity: (1) The first category consisted of 27 sub-
367 basins such as 32, 56, and 28, where the blue water scarcity level was the lowest (<20%). (2) The
368 second category comprised sub-basin 63, which has the most severe blue water scarcity (206%).
369 (3) The third category comprised seven sub-basins, such as 52, 58, and 60, all located in the lower
370 reaches, with relatively high blue water scarcity levels (40%-100%). These sub-basins are mostly
371 located in the tributaries of lower reaches, with a relatively large population and smaller river
372 streamflow compared to the mainstem of the Dongjiang River. (4) The fourth category consisted
373 of 28 sub-basins, such as 59, 62, and 8, with blue water scarcity levels ranging from 20% to 40%.
374 Similarly, hierarchical clustering was conducted for *GWSC*. When the standardized distance was
375 set to 500, *GWSC* in the sub-basins could be divided into three categories: (1) The first category
376 consisted of 56 sub-basins, such as 37, 56, and 29, with relatively low *GWSC* levels, all below
377 50%, indicating low *GWSC*. (2) The second category consisted of sub-basins 32 and 33, where the
378 predominant land use type was water areas, leading to higher *GWSC* due to high water surface
379 evaporation. (3) The third category consisted of sub-basins 47, 31, 54, 30, and 36, where the water
380 area proportion in these sub-basins was larger than in others, leading to significant influences from
381 water surface evaporation.



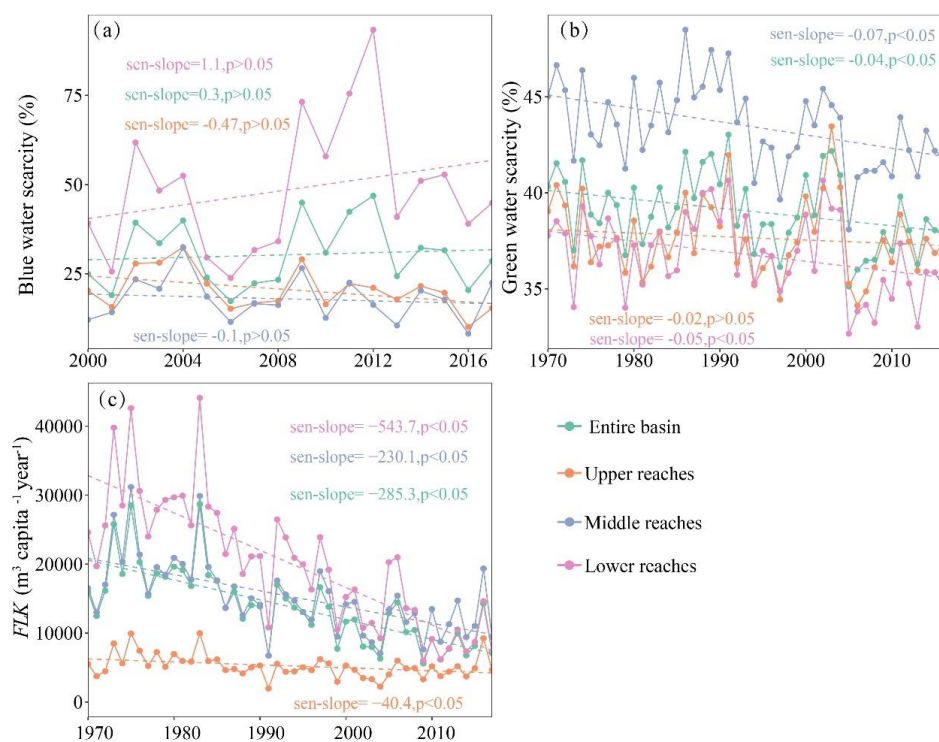
382
383 Figure 7. Hierarchical clustering tree of (a) *BWSC*, (b) *GWSC*.

384 The interannual variations in *BWSC* and *GWSC* in DRB showed distinct regional differences.

385 *BWSC* in the basin was slowly increasing at a rate of $0.3\% \text{ a}^{-1}$ (Fig. 8a). The *BWSC* in lower reaches
386 slowly increased at a rate of $1.1\% \text{ a}^{-1}$, while the *BWSC* in upper and middle reaches slowly
387 decreased at $-0.47\% \text{ a}^{-1}$ and $-0.1\% \text{ a}^{-1}$, respectively. *GWSC* in the upper, middle and lower reaches
388 of DRB showed a decreasing trend, with basin scale *GWSC* decreasing significantly at a rate of -
389 $0.04\% \text{ a}^{-1}$ (Fig. 8b). Despite the acceleration of urbanization and a significant increase in



390 population in the middle and lower reaches of the watershed, blue water availability and the
 391 amount of obtainable *BW* have been increasing. Additionally, the annual per capita water
 392 consumption in the basin has decreased from 481.0 m³ in 2000 to 245.0 m³ in 2020. As a result,
 393 the rate of increase in *BWSC* in the watershed has been relatively small. In contrast, the *GWF* in
 394 DRB demonstrated a significant decreasing trend, and the *GWS* increased slowly. Therefore, the
 395 *GWSC* in DRB demonstrated a significant decreasing trend. Meanwhile, the *FLK* index of the
 396 watershed showed a significant decreasing trend (-285.3 m³ per year), which means that the per
 397 capita water resources in the watershed have significantly decreased (Fig. 8c). This is due to the
 398 rapid population growth in the watershed and the slow increase in available water resources.



399
 400 Figure 8. Interannual variation of (a) *BWSC*, (b) *GWSC*, and (c) *FLK* index in DRB during 1970-2017.

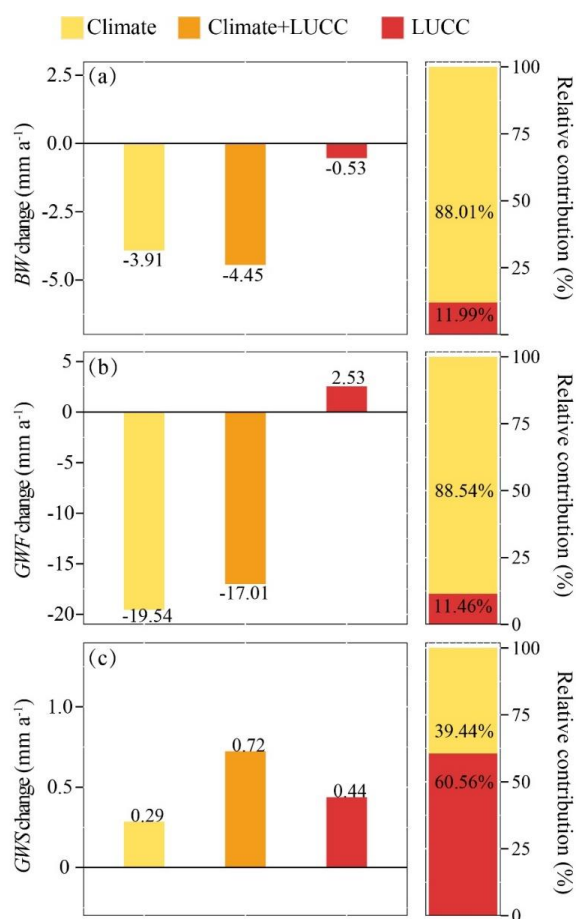


401 3.4 Impacts of LUCC and climate change on blue and green water

402 To examine the impacts of climate change and LUCC on *BW* and *GW* change, this study set
403 three climate conditions and land use scenarios to explore this effect by comparing the scenarios
404 (Table 3). The combined impacts of climate change and LUCC on *BW* and *GWS* in DRB were
405 superimposed, and the combined effect on *GWF* was a negatively synergistic effect. Figure 6
406 shows the variations in *BW* and *GW* under the impacts of climate change (S2-S1) and LUCC (S3-
407 S2), as well as their combined effects (S3-S1), along with the relative contribution of climate
408 change and LUCC to the *BW* and *GW* changes in DRB during 1970-2017. Under the joint
409 influences of climate change and LUCC, *BW* decreased by 4.5 mm a⁻¹. Among this decrease,
410 climate change resulted in a loss in *BW* of 3.9 mm a⁻¹, contributing 88.0%, while LUCC led to a
411 loss in *BW* of 0.5 mm a⁻¹, contributing 12.0% (Fig. 9a). The effect of climate change on *BW*
412 variation is much greater than that of LUCC at the basin scale. Under the combined influences of
413 climate change and LUCC, *GWF* decreased by 17.0 mm a⁻¹. Among this decrease, climate change
414 accounted for a decrease in *GWF* of 19.5 mm a⁻¹, contributing 88.5% to the decrease, while LUCC
415 led to an increase in *GWF* of 2.5 mm a⁻¹, contributing 11.5% (Fig. 9b). Overall, the influence of
416 climate change on *GWF* changes in the watershed is significantly more pronounced than that of
417 LUCC. Under the joint influences of climate change and LUCC, *GWS* increased by 0.7 mm a⁻¹.
418 Among this increase, climate change contributed to an increase in *GWS* of 0.3 mm a⁻¹, accounting
419 for 39.4%, while LUCC contributed to an increase in *GWS* of 0.4 mm a⁻¹, accounting for 60.6%



420 (Fig. 9c). DRB is situated in a humid regions with high *GWS*, resulting in small fluctuations of
421 *GWS* in response to precipitation changes. The fluctuations of *GWS* are primarily influenced by
422 the soil properties and land use. In general, the effect of climate change on the *GWS* change of
423 DRB is smaller than the effect of LUCC.



424
425 Figure 9. Effects and relative contribution of climate change and LUCC on the changes in (a) *BW*, (b) *GWF*,
426 (c) *GWS* in DRB during 1970 to 2017.

427 Under the coupled influences of climate change and LUCC, the *BW* and *GW* resources in
428 DRB have changed. However, there were differences in the joint impacts of climate change and



429 LUCC on BW and GW . Both climate change and LUCC have led to the decrease of BW in the
430 watershed, and the combined effect of climate change and LUCC on BW equals to the sum of their
431 individual effects. Climate change, such as a decrease in potential evapotranspiration, has resulted
432 in a decrease in GW in DRB, while LUCC has led to an increase in GW . Therefore, the joint
433 impacts of climate change and LUCC on GW was partially offset, resulting in the joint impacts
434 of climate change and LUCC on GW being less than the sum of their absolute individual effects.
435 Both climate change and LUCC have led to an increase in GWS in DRB, and the joint impacts of
436 climate change and LUCC on GWS equals to the sum of their individual effects.

437 **4 Discussion**

438 This study used the SWAT model to simulate the changes in BW and GW resources in DRB
439 over the past five decades and their response to climate change and LUCC. It also assessed the
440 water resource security in the basin. The results indicate that the total water resources showed a
441 decreasing trend in the past five decades in the entire DRB mainly due to decreases in precipitation,
442 which is similar to what Zhu et al. (2022) found. The findings also revealed that the GW exhibited
443 a decreasing trend, and the BW and GWS exhibited an increasing trend. Liu et al. (2010) similarly
444 found an increasing trend in annual surface runoff in DRB. Potential evapotranspiration and solar
445 radiation in DRB showed a decreasing trend, which may be the main cause of the significant
446 decrease in GW in the basin (Fig. S2), and similar conclusions are obtained in He et al. (2013).



447 We show that water resources in DRB are dominated by *BW*, with a mean annual *GWI* of 0.4,
448 which is the same as what many studies show in humid areas (Nie et al., 2023). Although the *GWI*
449 in humid areas is much smaller than that in arid areas, the ratio of *GW* in DRB still reach 40%, so
450 it is imperative to incorporate *GW* in the water resources assessment system. The *GWI* in the upper
451 and middle reaches of DRB exceeded 0.4, while that in the lower reaches was only about 0.3.
452 These results mean that to ensure the appropriate utilization of water resources, effective water
453 management in the upper and middle reaches of DRB should consider *GW* planning while water
454 management in the lower reaches should mainly consider *BW*. The assessment results of *BWSC*
455 and *GWSC* in DRB similarly illustrates this issue. The *GWSC* in the upper and middle reaches was
456 bigger than that in the lower reaches of DRB, while the *BWSC* in the lower reaches of DRB was
457 bigger than in the upper and middle reaches (Fig. 8).

458 There are robust correlations between *BW* and precipitation, *GWF* and potential
459 evapotranspiration in DRB. Climate change plays a dominant role in variations of *BW* and *GWF*.
460 *BW* is more sensitive to precipitation and potential evapotranspiration. *GWF* shows sensitivity to
461 changes in potential evapotranspiration and *GWS* is influenced by both precipitation and potential
462 evapotranspiration (He et al., 2015; Jeyrani et al., 2021). Of course, there are also studies for arid
463 regions show that *GWF* is mainly affected by precipitation (Jun Wu et al., 2021), which may be
464 linked to the hydrothermal conditions of the basin. There is sufficient precipitation in DRB, where
465 the *GWF* changes are mainly energy-limited, and effect of precipitation on the *GWF* are smaller.



466 Although *BW* and *GW* are mainly affected by climate change, the influences of LUCC on
467 them cannot be ignored. The reaction of water resources to LUCC is exceedingly intricate and
468 involves various hydrological processes, including runoff yield, infiltration, and groundwater (Cuo,
469 2016; Zhang and Shangguan, 2016). As there is a strong compensatory effect of diverse land use
470 in the hydrological system, particularly in expansive watersheds, this could create a strong
471 resistance to *GW* and *BW* conversion (Lin et al., 2015). Decrease in forest land or increase in
472 cultivated and urban land could lead to an rise in *BW* and a decline in *GW* in the watershed. Veettil
473 and Mishra (2018) demonstrate that there is a 10% rise in forest land cover and a 1.4% drop in *BW*,
474 indicating a negative elasticity between the two. However, the effect of urban land on streamflow
475 in different time periods showed the opposite effect. On the one hand, the increase in urban land
476 results in increases in impermeable area and thus surface runoff in the basin, but at the same time,
477 the increase in urban land may also reduce groundwater discharge to streamflow. At the same time,
478 LUCC often results in changes in vegetation. Vegetation variations affect the water cycle by
479 altering canopy interception (Shao et al., 2018; Jianping Wu et al., 2019), transpiration (Chen et
480 al., 2023) and canopy evaporation, and ameliorating soil structure (Qiu et al., 2022), Thus
481 increasing vegetation often increases infiltration and soil moisture and reduces surface runoff.

482 There are several limitations and uncertainties in this research. (1) Since the quantity of the
483 *BW* and *GW* is derived from the output results of the model simulations, including water yield, *ET*,
484 soil moisture, and groundwater, the precision of the outcomes depends largely on the precision of



485 the model simulations. Given the absence of observed evapotranspiration and soil moisture data
486 for DRB, this study calibrated and validated the SWAT model using only monthly streamflow,
487 which may weaken these results to some extent. To enhance the credibility of the model, this study
488 also utilized widely used actual evapotranspiration data (GLEAM) and soil moisture (ERA5-land)
489 during model validation at a basin scale. The findings indicated that the simulation performance is
490 relatively good and meets the accuracy requirements for simulation. (2) Climate change, LUCC,
491 and large reservoir operation are the primary factors influencing the changes in hydrological
492 conditions in DRB. The contributions of reservoir regulation, LUCC, water resource utilization,
493 and climate change to the distribution of intra-annual flow are 33.5%, -9%, 4.5%, and 1%,
494 respectively, during 1956-2009 (Tu et al., 2015). The operation of reservoirs, including large
495 reservoirs like the Xinfengjiang Reservoir, is one of the important reasons for hydrological changes
496 in DRB (Lin et al., 2014; Zhang et al., 2015). The reservoir module was not established when
497 constructing the SWAT model in this research. To obtain natural *BW* and *GW* volumes in the
498 watershed and mitigate the impact of hydraulic engineering, reconstructed natural streamflow
499 based on observed flow was utilized for model calibration and validation. However, hydraulic
500 engineering significantly influences the annual allocation of *BW*. The flow restoration considered
501 the impacts of the three major reservoirs on the Dongjiang River and did not consider the impacts
502 of other minor hydraulic projects and human water consumption. (3) Both the calculations of
503 *BWSC* and the *FLK* index include environmental flows. This study represented the proportion of



504 environmental flow in streamflow as 80%. Some studies have suggested that assuming
505 environmental flow to be 80% of the total water resources in a basin may overestimate water
506 scarcity (Liu et al., 2017; Richter et al., 2012). Therefore, we varied the proportion of
507 environmental flow and assessed the degree of *BWSC* using 60% and 70% proportions. Results
508 show that only the 63rd sub-basin changed from severe *BWSC* to moderate to high *BWSC*, while
509 other sub-basins remained with low *BWSC*. Therefore, the threshold for environmental flow has a
510 minor impact on this paper. The assessment of *BWSC* and per capita water resources did not take
511 into account the water demand of cities such as Shenzhen and Hong Kong, although the water
512 supply for these cities primarily comes from the Dongjiang River through the Dongjiang-Shenzhen
513 Water Supply Project. (4) The hydrological modeling approach utilized in this research is a
514 frequently used method for quantitative analysis of attribution. Nevertheless, it implies
515 independence between climate change and LUCC and does not adequately distinguish the impacts
516 of these two components. Such restriction is diffusely recognized to exist (Dey and Mishra, 2017).
517 Despite this recognized limitation, hydrological modeling methods have been widely used in
518 numerous similar researches, yielding credible results (Li et al., 2021; Nie et al., 2023).

519 **5 Conclusion**

520 This study analyzed the spatio-temporal evolution of *BW* and *GW*, assessed the water security,
521 and evaluated the effects of climate change and LUCC on *BW* and *GW* in DRB using the SWAT



522 model. The conclusions can be outlined as follows:

523 (1) During 1970-2017, grass land, cultivated land, and forestland in DRB decreased by 4.3%,
524 10.8%, and 0.2%, respectively, while urban land and water areas increased by 137% and 2.8%,
525 respectively. The annual precipitation and potential evapotranspiration showed a non-significant
526 decreasing trend, while the annual average temperature showed a significantly increasing trend.

527 (2) The annual *BW*, *GWF*, and green storage in DRB from 1970-2017 were 1240.8 mm, 840.7
528 mm, and 151.4mm, respectively. *BW* (0.14 mm a^{-1}) and *GWS* (0.015 mm a^{-1}) in DRB showed no
529 significant increasing trend, and *GWF* (-0.57 mm a^{-1}) showed a significant decreasing trend.

530 (3) The level of annual *BWSC* and *GWSC* in DRB were low, and per capita water resources
531 exceeded $1,700 \text{ m}^3 \text{ capita}^{-1} \text{ a}^{-1}$. *BWSC* displayed a non-significant increasing trend, while the
532 *GWSC* and *FLK* index displayed a significant decreasing trend, especially in lower reaches.

533 (4) Climate change was the major driving factor of changes in *BW* and *GWF*, and LUCC was
534 the major driving factor of *GWS* change. Climate change contributed to 88.0%, 88.5%, and 39.4%
535 of the changes in *BW*, *GWF*, and *GWS* in DRB, respectively. Both climate change and LUCC
536 decrease *BW*, while climate change (LUCC) decrease (increase) *GW* flow in DRB.

537 **Competing interests**

538 The contact author has declared that none of the authors has any competing interests.



539 **Acknowledgments**

540 This study was supported by the National Key Research and Development Program of China
541 (2021YFC3001000), the Science and Technology Innovation Program from Water Resources of
542 Guangdong Province (2023-01), and the National Natural Science Foundation of China (52179029,
543 52179030).



References

- Acero Triana, J.S., Ajami, H., 2022. Identifying Major Hydrologic Change Drivers in a Highly Managed Transboundary Endorheic Basin: Integrating Hydro-Ecological Models and Time Series Data Mining Techniques. *Water Resources Research* 58, e2022WR032281. <https://doi.org/10.1029/2022WR032281>
- Aghakhani Afshar, A., Hassanzadeh, Y., Pourreza-Bilondi, M., Ahmadi, A., 2018. Analyzing long-term spatial variability of blue and green water footprints in a semi-arid mountainous basin with MIROC-ESM model (case study: Kashafrood River Basin, Iran). *Theoretical and Applied Climatology* 134, 885–899. <https://doi.org/10.1007/s00704-017-2309-0>
- Arnold, J.G., Srinivasan, R., Muttiah, R.S., Williams, J.R., 1998. Large Area Hydrologic Modeling and Assessment Part I: Model Development1. *JAWRA Journal of the American Water Resources Association* 34, 73–89. <https://doi.org/10.1111/j.1752-1688.1998.tb05961.x>
- Arshad, A., Mirchi, A., Samimi, M., Ahmad, B., 2022. Combining downscaled-GRACE data with SWAT to improve the estimation of groundwater storage and depletion variations in the Irrigated Indus Basin (IIB). *Science of The Total Environment* 838, 156044. <https://doi.org/10.1016/j.scitotenv.2022.156044>
- Bai, X., Jia, X., Jia, Y., Shao, M., Hu, W., 2020. Modeling long-term soil water dynamics in response to land-use change in a semi-arid area. *Journal of Hydrology* 585, 124824. <https://doi.org/10.1016/j.jhydrol.2020.124824>
- Chagas, V.B.P., Chaffe, P.L.B., Blöschl, G., 2022. Climate and land management accelerate the Brazilian water cycle. *Nat Commun* 13, 5136. <https://doi.org/10.1038/s41467-022-32580-x>
- Chen, Z., Wang, W., Cescatti, A., Forzieri, G., 2023. Climate-driven vegetation greening further reduces water availability in drylands. *Global Change Biology* 29, 1628–1647. <https://doi.org/10.1111/gcb.16561>
- Chouchane, H., Krol, M.S., Hoekstra, A.Y., 2020. Changing global cropping patterns to minimize national blue water scarcity. *Hydrology and Earth System Sciences* 24, 3015–3031. <https://doi.org/10.5194/hess-24-3015-2020>
- Cook, B.I., Smerdon, J.E., Seager, R., Coats, S., 2014. Global warming and 21 st century drying. *Climate Dynamics* 43, 2607–2627. <https://doi.org/10.1007/s00382-014-2075-y>
- Cooper, C.M., Troutman, J.P., Awal, R., Habibi, H., Fares, A., 2022. Climate change-induced variations in blue and green water usage in U.S. urban agriculture. *Journal of Cleaner Production* 348, 131326. <https://doi.org/10.1016/j.jclepro.2022.131326>
- Cuo, L., 2016. Land use/cover change impacts on hydrology in large river basins: a review. *Terrestrial Water Cycle and Climate Change: Natural and Human-Induced Impacts* 221, 103. <https://doi.org/10.1002/9781118971772.ch6>
- Dai, C., Qin, X., Dong, F., Cai, Y., 2022. Climate change impact on blue and green water resources distributions in the Beijiing River basin based on CORDEX projections. *Journal of Water*



- and Climate Change 13, 2780–2798. <https://doi.org/10.2166/wcc.2022.115>
- Dey, P., Mishra, A., 2017. Separating the impacts of climate change and human activities on streamflow: A review of methodologies and critical assumptions. *Journal of Hydrology* 548, 278–290. <https://doi.org/10.1016/j.jhydrol.2017.03.014>
- Eekhout, J.P.C., Hunink, J.E., Terink, W., de Vente, J., 2018. Why increased extreme precipitation under climate change negatively affects water security. *Hydrology and Earth System Sciences* 22, 5935–5946. <https://doi.org/10.5194/hess-22-5935-2018>
- Falkenmark, M., Folke, C., Falkenmark, Malin, 2003. Freshwater as shared between society and ecosystems: from divided approaches to integrated challenges. *Philosophical Transactions of the Royal Society of London. Series B: Biological Sciences* 358, 2037–2049. <https://doi.org/10.1098/rstb.2003.1386>
- Falkenmark, M., Lundqvist, J., Widstrand, C., 1989. Macro-scale water scarcity requires micro-scale approaches. *Natural Resources Forum* 13, 258–267. <https://doi.org/10.1111/j.1477-8947.1989.tb00348.x>
- Falkenmark, M., Rockström, J., 2006. The New Blue and Green Water Paradigm: Breaking New Ground for Water Resources Planning and Management. *Journal of Water Resources Planning and Management* 132, 129–132. [https://doi.org/10.1061/\(ASCE\)0733-9496\(2006\)132:3\(129\)](https://doi.org/10.1061/(ASCE)0733-9496(2006)132:3(129))
- Farr, T.G., Rosen, P.A., Caro, E., Crippen, R., Duren, R., Hensley, S., Kobrick, M., Paller, M., Rodriguez, E., Roth, L., Seal, D., Shaffer, S., Shimada, J., Umland, J., Werner, M., Oskin, M., Burbank, D., Alsdorf, D., 2007. The Shuttle Radar Topography Mission. *Reviews of Geophysics* 45. <https://doi.org/10.1029/2005RG000183>
- Ficklin, D.L., Robeson, S.M., Knouft, J.H., 2016. Impacts of recent climate change on trends in baseflow and stormflow in United States watersheds. *Geophys Res Lett* 43, 5079–5088. <https://doi.org/10.1002/2016gl069121>
- Fischer, G., Nachtergaele, F., Prieler, S., Van Velthuizen, H.T., Verelst, L., Wiberg, D., 2008. Global agro-ecological zones assessment for agriculture (GAEZ 2008). IIASA, Laxenburg, Austria and FAO, Rome, Italy 10.
- Foley, J.A., DeFries, R., Asner, G.P., Barford, C., Bonan, G., Carpenter, S.R., Chapin, F.S., Coe, M.T., Daily, G.C., Gibbs, H.K., 2005. Global consequences of land use. *Science* 309, 570–574. <https://doi.org/10.1126/science.1111772>
- Han, Z., Huang, S., Huang, Q., Bai, Q., Leng, G., Wang, H., Zhao, J., Wei, X., Zheng, X., 2020. Effects of vegetation restoration on groundwater drought in the Loess Plateau, China. *Journal of Hydrology* 591, 125566. <https://doi.org/10.1016/j.jhydrol.2020.125566>
- He, Y., Lin, K., Chen, X., 2013. Effect of Land Use and Climate Change on Runoff in the Dongjiang Basin of South China. *Mathematical Problems in Engineering* 2013, e471429. <https://doi.org/10.1155/2013/471429>
- He, Y., Lin, K., Chen, X., Ye, C., Cheng, L., 2015. Classification-Based Spatiotemporal Variations of Pan Evaporation Across the Guangdong Province, South China. *Water Resour Manage* 29, 901–912. <https://doi.org/10.1007/s11269-014-0850-5>
- Hoek van Dijke, A.J., Herold, M., Mallick, K., Benedict, I., Machwitz, M., Schlerf, M., Pranindita, A., Theeuwes, J.J.E., Bastin, J.-F., Teuling, A.J., 2022. Shifts in regional water availability



- due to global tree restoration. *Nature Geoscience* 15, 363–368. <https://doi.org/10.1038/s41561-022-00935-0>
- Hoekstra, A.Y., Mekonnen, M.M., Chapagain, A.K., Mathews, R.E., Richter, B.D., 2012. Global Monthly Water Scarcity: Blue Water Footprints versus Blue Water Availability. *PLOS ONE* 7, e32688. <https://doi.org/10.1371/journal.pone.0032688>
- Honrado, J.P., Vieira, C., Soares, C., Monteiro, M.B., Marcos, B., Pereira, H.M., Partidário, M.R., 2013. Can we infer about ecosystem services from EIA and SEA practice? A framework for analysis and examples from Portugal. *Environmental Impact Assessment Review, Ecosystem services in EIA and SEA* 40, 14–24. <https://doi.org/10.1016/j.eiar.2012.12.002>
- Huang, H., Xue, Y., Chilukoti, N., Liu, Y., Chen, G., Diallo, I., 2020. Assessing Global and Regional Effects of Reconstructed Land-Use and Land-Cover Change on Climate since 1950 Using a Coupled Land–Atmosphere–Ocean Model. *Journal of Climate* 33, 8997–9013. <https://doi.org/10.1175/JCLI-D-20-0108.1>
- Huang, Y., Cai, Y., Xie, Y., Zhang, F., He, Y., Zhang, P., Li, Bowen, Li, Bo, Jia, Q., Wang, Y., Qi, Z., 2022. An optimization model for water resources allocation in Dongjiang River Basin of Guangdong-Hong Kong-Macao Greater Bay Area under multiple complexities. *Science of The Total Environment* 820, 153198. <https://doi.org/10.1016/j.scitotenv.2022.153198>
- Jeyrani, F., Morid, S., Srinivasan, R., 2021. Assessing basin blue–green available water components under different management and climate scenarios using SWAT. *Agricultural Water Management* 256, 107074. <https://doi.org/10.1016/j.agwat.2021.107074>
- Jiang, J., Wang, Z., Lai, C., Wu, X., Chen, X., 2023. Climate and landuse change enhance spatio-temporal variability of Dongjiang river flow and ammonia nitrogen. *Science of The Total Environment* 867, 161483. <https://doi.org/10.1016/j.scitotenv.2023.161483>
- Konapala, G., Mishra, A.K., Wada, Y., Mann, M.E., 2020. Climate change will affect global water availability through compounding changes in seasonal precipitation and evaporation. *Nat Commun* 11, 3044. <https://doi.org/10.1038/s41467-020-16757-w>
- Lee, X., Goulden, M.L., Hollinger, D.Y., Barr, A., Black, T.A., Bohrer, G., Bracho, R., Drake, B., Goldstein, A., Gu, L., 2011. Observed increase in local cooling effect of deforestation at higher latitudes. *Nature* 479, 384–387. <https://doi.org/10.1038/nature10588>
- Li, C., Tang, G., Hong, Y., 2018. Cross-evaluation of ground-based, multi-satellite and reanalysis precipitation products: Applicability of the Triple Collocation method across Mainland China. *Journal of Hydrology* 562, 71–83. <https://doi.org/10.1016/j.jhydrol.2018.04.039>
- Li, X., Zhang, Y., Ma, N., Li, C., Luan, J., 2021. Contrasting effects of climate and LULC change on blue water resources at varying temporal and spatial scales. *Science of The Total Environment* 786, 147488. <https://doi.org/10.1016/j.scitotenv.2021.147488>
- Lian, X., Piao, S., Li, L.Z.X., Li, Y., Huntingford, C., Ciais, P., Cescatti, A., Janssens, I.A., Peñuelas, J., Buermann, W., Chen, A., Li, X., Myneni, R.B., Wang, X., Wang, Y., Yang, Y., Zeng, Z., Zhang, Y., McVicar, T.R., 2020. Summer soil drying exacerbated by earlier spring greening of northern vegetation. *Science Advances* 6, eaax0255. <https://doi.org/10.1126/sciadv.aax0255>
- Liang, J., He, X., Zeng, G., Zhong, M., Gao, X., Li, Xin, Li, Xiaodong, Wu, H., Feng, C., Xing,



- W., 2018. Integrating priority areas and ecological corridors into national network for conservation planning in China. *Science of the Total Environment* 626, 22–29.
- Liang, J., Liu, Q., Zhang, H., Li, Xiaodong, Qian, Z., Lei, M., Li, Xin, Peng, Y., Li, S., Zeng, G., 2020. Interactive effects of climate variability and human activities on blue and green water scarcity in rapidly developing watershed. *Journal of Cleaner Production* 265, 121834. <https://doi.org/10.1016/j.jclepro.2020.121834>
- Lin, B., Chen, X., Yao, H., Chen, Y., Liu, M., Gao, L., James, A., 2015. Analyses of landuse change impacts on catchment runoff using different time indicators based on SWAT model. *Ecological Indicators* 58, 55–63. <https://doi.org/10.1016/j.ecolind.2015.05.031>
- Lin, K., Lian, Y., Chen, X., Lu, F., 2014. Changes in runoff and eco-flow in the Dongjiang River of the Pearl River Basin, China. *Front. Earth Sci.* 8, 547–557. <https://doi.org/10.1007/s11707-014-0434-y>
- Liu, B., Peng, S., Liao, Y., Long, W., 2018. The causes and impacts of water resources crises in the Pearl River Delta. *Journal of Cleaner Production* 177, 413–425. <https://doi.org/10.1016/j.jclepro.2017.12.203>
- Liu, D., Chen, X., Lian, Y., Lou, Z., 2010. Impacts of climate change and human activities on surface runoff in the Dongjiang River basin of China. *Hydrological Processes* 24, 1487–1495. <https://doi.org/10.1002/hyp.7609>
- Liu, J., Yang, H., Gosling, S.N., Kumm, M., Flörke, M., Pfister, S., Hanasaki, N., Wada, Y., Zhang, X., Zheng, C., Alcamo, J., Oki, T., 2017. Water scarcity assessments in the past, present, and future. *Earth's Future* 5, 545–559. <https://doi.org/10.1002/2016EF000518>
- Martens, B., Miralles, D.G., Lievens, H., Fernández-Prieto, D., Beck, H.E., Dorigo, W.A., Verhoest, N.E.C., 2017. GLEAM v3: satellite-based land evaporation and root-zone soil moisture. *Geoscientific Model Development* 10, 1903–1925. <https://doi.org/10.5194/gmd-10-1903-2017>
- Martínez-Salvador, A., Conesa-García, C., 2020. Suitability of the SWAT Model for Simulating Water Discharge and Sediment Load in a Karst Watershed of the Semiarid Mediterranean Basin. *Water Resour Manage* 34, 785–802. <https://doi.org/10.1007/s11269-019-02477-4>
- Mohan, M., Kandya, A., 2015. Impact of urbanization and land-use/land-cover change on diurnal temperature range: A case study of tropical urban airshed of India using remote sensing data. *Science of the Total Environment* 506, 453–465. <https://doi.org/10.1016/j.scitotenv.2014.11.006>
- Muñoz Sabater, J., 2019. ERA5-Land monthly averaged data from 1981 to present, Copernicus Climate Change Service (C3S) Climate Data Store (CDS).
- Nearing, M.A., Jetten, V., Baffaut, C., Cerdan, O., Couturier, A., Hernandez, M., Le Bissonnais, Y., Nichols, M.H., Nunes, J.P., Renschler, C.S., 2005. Modeling response of soil erosion and runoff to changes in precipitation and cover. *CATENA* 61, 131–154. <https://doi.org/10.1016/j.catena.2005.03.007>
- Neitsch, S., Arnold, J., Kiniry, J., Williams, J., King, K., 2002. Soil and water assessment tool (SWAT): theoretical documentation, version 2000. Texas Water Resources Institute, College Station, Texas, TWRI Report TR-191.



- Nie, N., Li, T., Miao, Y., Zhang, W., Gao, H., He, H., Zhao, D., Liu, M., 2023. Asymmetry of blue and green water changes in the Yangtze river basin, China, examined by multi-water-variable calibrated SWAT model. *Journal of Hydrology* 625, 130099. <https://doi.org/10.1016/j.jhydrol.2023.130099>
- Pandey, B.K., Khare, D., Kawasaki, A., Mishra, P.K., 2019. Climate Change Impact Assessment on Blue and Green Water by Coupling of Representative CMIP5 Climate Models with Physical Based Hydrological Model. *Water Resour Manage* 33, 141–158. <https://doi.org/10.1007/s11269-018-2093-3>
- Pokhrel, Y., Felfelani, F., Satoh, Y., Boulange, J., Burek, P., Gädeke, A., Gerten, D., Gosling, S.N., Grillakis, M., Gudmundsson, L., Hanasaki, N., Kim, H., Koutroulis, A., Liu, J., Papadimitriou, L., Schewe, J., Müller Schmied, H., Stacke, T., Telteu, C.-E., Thiery, W., Veldkamp, T., Zhao, F., Wada, Y., 2021. Global terrestrial water storage and drought severity under climate change. *Nat. Clim. Chang.* 11, 226–233. <https://doi.org/10.1038/s41558-020-00972-w>
- Qiu, D., Xu, R., Wu, C., Mu, X., Zhao, G., Gao, P., 2023. Effects of vegetation restoration on soil infiltrability and preferential flow in hilly gully areas of the Loess Plateau, China. *CATENA* 221, 106770. <https://doi.org/10.1016/j.catena.2022.106770>
- Qiu, D., Xu, R., Wu, C., Mu, X., Zhao, G., Gao, P., 2022. Vegetation restoration improves soil hydrological properties by regulating soil physicochemical properties in the Loess Plateau, China. *Journal of Hydrology* 609, 127730. <https://doi.org/10.1016/j.jhydrol.2022.127730>
- Richter, B.D., 2010. Re-thinking environmental flows: from allocations and reserves to sustainability boundaries. *River Research and Applications* 26, 1052–1063. <https://doi.org/10.1002/rra.1320>
- Richter, B.D., Davis, M.M., Apse, C., Konrad, C., 2012. A Presumptive Standard for Environmental Flow Protection. *River Research and Applications* 28, 1312–1321. <https://doi.org/10.1002/rra.1511>
- Schewe, J., Heinke, J., Gerten, D., Haddeland, I., Arnell, N.W., Clark, D.B., Dankers, R., Eisner, S., Fekete, B.M., Colón-González, F.J., Gosling, S.N., Kim, H., Liu, X., Masaki, Y., Portmann, F.T., Satoh, Y., Stacke, T., Tang, Q., Wada, Y., Wisser, D., Albrecht, T., Frieler, K., Piontek, F., Warszawski, L., Kabat, P., 2014. Multimodel assessment of water scarcity under climate change. *Proceedings of the National Academy of Sciences* 111, 3245–3250. <https://doi.org/10.1073/pnas.1222460110>
- Schuol, J., Abbaspour, K.C., Yang, H., Srinivasan, R., Zehnder, A.J., 2008. Modeling blue and green water availability in Africa. *Water resources research* 44.
- Schyns, J.F., Hoekstra, A.Y., Booij, M.J., Hogeboom, R.J., Mekonnen, M.M., 2019. Limits to the world's green water resources for food, feed, fiber, timber, and bioenergy. *Proceedings of the National Academy of Sciences* 116, 4893–4898. <https://doi.org/10.1073/pnas.1817380116>
- Shao, M., Wang, Y., Xia, Y., Jia, X., 2018. Soil drought and water carrying capacity for vegetation in the critical zone of the Loess Plateau: A review. *Vadose Zone Journal* 17, 1539–1663. <https://doi.org/10.2136/vzj2017.04.0077>
- Shen, Q., Cong, Z., Lei, H., 2017. Evaluating the impact of climate and underlying surface change on runoff within the Budyko framework: A study across 224 catchments in China. *Journal of*



- Hydrology 554, 251–262. <https://doi.org/10.1016/j.jhydrol.2017.09.023>
- Sherwood, S., Fu, Q., 2014. A drier future? *Science* 343, 737–739. <https://doi.org/10.1126/science.1247620>
- Stocker, B.D., Tumber-Dávila, S.J., Konings, A.G., Anderson, M.C., Hain, C., Jackson, R.B., 2023. Global patterns of water storage in the rooting zones of vegetation. *Nat. Geosci.* 1–7. <https://doi.org/10.1038/s41561-023-01125-2>
- Tan, X., Gan, T.Y., 2015. Contribution of human and climate change impacts to changes in streamflow of Canada. *Sci Rep* 5, 17767. <https://doi.org/10.1038/srep17767>
- Tan, Xuezhi, Wu, X., Huang, Z., Deng, S., Hu, M., Yew Gan, T., 2022. Detection and attribution of the decreasing precipitation and extreme drought 2020 in southeastern China. *Journal of Hydrology* 610, 127996. <https://doi.org/10.1016/j.jhydrol.2022.127996>
- Tan, Xuejin, Liu, B., Tan, Xuezhi, 2020. Global Changes in Baseflow Under the Impacts of Changing Climate and Vegetation. *Water Resources Research* 56, e2020WR027349. <https://doi.org/10.1029/2020WR027349>
- Tan, Xuejin, Liu, B., Tan, Xuezhi, Chen, X., 2022. Long-Term Water Imbalances of Watersheds Resulting From Biases in Hydroclimatic Data Sets for Water Budget Analyses. *Water Resources Research* 58, e2021WR031209. <https://doi.org/10.1029/2021WR031209>
- Tan, Xuejin, Tan, Xuezhi, Liu, B., Huang, Z., 2023. Contribution of changes in vegetation composition and climate variability on streamflow across the global watersheds. *CATENA* 232, 107394. <https://doi.org/10.1016/j.catena.2023.107394>
- Tao, S., Fang, J., Ma, S., Cai, Q., Xiong, X., Tian, D., Zhao, X., Fang, L., Zhang, H., Zhu, J., Zhao, S., 2020. Changes in China's lakes: climate and human impacts. *National Science Review* 7, 132–140. <https://doi.org/10.1093/nsr/nwz103>
- Tu, X., Singh, V.P., Chen, X., Chen, L., Zhang, Q., Zhao, Y., 2015. Intra-annual Distribution of Streamflow and Individual Impacts of Climate Change and Human Activities in the Dongjiang River Basin, China. *Water Resour Manage* 29, 2677–2695. <https://doi.org/10.1007/s11269-015-0963-5>
- Tu, X., Wu, H., Singh, V.P., Chen, X., Lin, K., Xie, Y., 2018. Multivariate design of socioeconomic drought and impact of water reservoirs. *Journal of Hydrology* 566, 192–204. <https://doi.org/10.1016/j.jhydrol.2018.09.012>
- Vano, J.A., Das, T., Lettenmaier, D.P., 2012. Hydrologic sensitivities of Colorado River runoff to changes in precipitation and temperature. *Journal of Hydrometeorology* 13, 932–949. <https://doi.org/10.1175/JHM-D-11-069.1>
- Veettil, A.V., Mishra, A., 2020. Water Security Assessment for the Contiguous United States Using Water Footprint Concepts. *Geophysical Research Letters* 47, e2020GL087061. <https://doi.org/10.1029/2020GL087061>
- Veettil, A.V., Mishra, A.K., 2018. Potential influence of climate and anthropogenic variables on water security using blue and green water scarcity, Falkenmark index, and freshwater provision indicator. *Journal of Environmental Management* 228, 346–362. <https://doi.org/10.1016/j.jenvman.2018.09.012>
- Veettil, A.V., Mishra, A.K., 2016. Water security assessment using blue and green water footprint



- concepts. *Journal of Hydrology* 542, 589–602. <https://doi.org/10.1016/j.jhydrol.2016.09.032>
- Walters, K.M., Babbar-Sebens, M., 2016. Using climate change scenarios to evaluate future effectiveness of potential wetlands in mitigating high flows in a Midwestern US watershed. *Ecological engineering* 89, 80–102. <https://doi.org/10.1016/j.ecoleng.2016.01.014>
- Wu, Jiefeng, Chen, X., Yu, Z., Yao, H., Li, W., Zhang, D., 2019. Assessing the impact of human regulations on hydrological drought development and recovery based on a ‘simulated-observed’ comparison of the SWAT model. *Journal of Hydrology* 577, 123990. <https://doi.org/10.1016/j.jhydrol.2019.123990>
- Wu, Jiefeng, Chen, X., Yuan, X., Yao, H., Zhao, Y., AghaKouchak, A., 2021. The interactions between hydrological drought evolution and precipitation-streamflow relationship. *Journal of Hydrology* 597, 126210. <https://doi.org/10.1016/j.jhydrol.2021.126210>
- Wu, Jun, Deng, G., Zhou, D., Zhu, X., Ma, J., Cen, G., Jin, Y., Zhang, J., 2021. Effects of climate change and land-use changes on spatiotemporal distributions of blue water and green water in Ningxia, Northwest China. *J. Arid Land* 13, 674–687. <https://doi.org/10.1007/s40333-021-0074-5>
- Wu, Jianping, Liu, L., Sun, C., Su, Y., Wang, C., Yang, J., Liao, J., He, X., Li, Q., Zhang, C., Zhang, H., 2019. Estimating Rainfall Interception of Vegetation Canopy from MODIS Imageries in Southern China. *Remote Sensing* 11, 2468. <https://doi.org/10.3390/rs11212468>
- Xin, Z., Li, Y., Zhang, L., Ding, W., Ye, L., Wu, J., Zhang, C., 2019. Quantifying the relative contribution of climate and human impacts on seasonal streamflow. *Journal of Hydrology* 574, 936–945. <https://doi.org/10.1016/j.jhydrol.2019.04.095>
- Xu, X., 2017. China population spatial distribution kilometer grid dataset. Data Registration and Publishing System of Resource and Environmental Science Data Center of Chinese Academy of Sciences.
- Xu, X., Liu, J., Zhang, S., Li, R., Yan, C., Wu, S., 2018. Multi-period land use land cover remote sensing monitoring dataset in China (CNLUCC). Resource and Environmental Science Data Registration and Publication System. (<http://www.resdc.cn/DOI>). <https://doi.org/DOI:10.12078/2018070201>
- Yang, L.E., Chan, F.K.S., Scheffran, J., 2018. Climate change, water management and stakeholder analysis in the Dongjiang River basin in South China. *International Journal of Water Resources Development* 34, 166–191. <https://doi.org/10.1080/07900627.2016.1264294>
- Zang, C., Liu, J., 2013. Trend analysis for the flows of green and blue water in the Heihe River basin, northwestern China. *Journal of Hydrology* 502, 27–36. <https://doi.org/10.1016/j.jhydrol.2013.08.022>
- Zhang, Q., Gu, X., Singh, V.P., Chen, X., 2015. Evaluation of ecological instream flow using multiple ecological indicators with consideration of hydrological alterations. *Journal of Hydrology* 529, 711–722. <https://doi.org/10.1016/j.jhydrol.2015.08.066>
- Zhang, Y., Shangguan, Z., 2016. The change of soil water storage in three land use types after 10years on the Loess Plateau. *CATENA* 147, 87–95. <https://doi.org/10.1016/j.catena.2016.06.036>
- Zhang, Yongyong, Xia, J., Yu, J., Randall, M., Zhang, Yichi, Zhao, T., Pan, X., Zhai, X., Shao, Q.,



2018. Simulation and assessment of urbanization impacts on runoff metrics: insights from landuse changes. *Journal of Hydrology* 560, 247–258. <https://doi.org/10.1016/j.jhydrol.2018.03.031>
- Zhu, K., Qiu, X., Luo, Y., Dai, M., Lu, X., Zang, C., Zhang, W., Gan, X., Zhula, W., 2022. Spatial and temporal dynamics of water resources in typical ecosystems of the Dongjiang River Basin, China. *Journal of Hydrology* 614, 128617. <https://doi.org/10.1016/j.jhydrol.2022.128617>
- Zuo, D., Xu, Z., Peng, D., Song, J., Cheng, L., Wei, S., Abbaspour, K.C., Yang, H., 2015. Simulating spatiotemporal variability of blue and green water resources availability with uncertainty analysis. *Hydrological Processes* 29, 1942–1955.